Increased fluid flow activity in shallow sediments at the 3-km long Hugin Fracture in the Central North Sea

A. Lichtschlag[1*] , M. Cevatoglu[2+], D.P. Connelly[1], R.H. James[1,2] and J.M. Bull[2]

[1] National Oceanography Centre, University of Southampton Waterfront Campus, Southampton, UK.

[2] Ocean and Earth Science, University of Southampton, National Oceanography Centre Southampton, Southampton, UK.

*Corresponding author: Anna Lichtschlag, a.lichtschlag@noc.ac.uk

+Current address: Fugro Sial Geosciences Consulting and Engineering, Istanbul, Turkey

Key Points:

- *We provide evidence for fluid flow within shallow sediments at the Hugin Fracture in the Central North Sea*

- *Shallow sediment porewaters have two different sources*

- *Seismic amplitude anomalies show a bright spot in the shallow sediments that is indicative of the presence of gas-rich fluids at a fault bend*

Abstract

The North Sea hosts a wide variety of seafloor seeps that may be important for transfer of chemical species, such as methane, from the Earth's interior to its exterior. Here we provide geochemical and geophysical evidence for fluid flow within shallow sediments at the recently discovered, 3-km long Hugin Fracture in the Central North Sea. Although venting of gas bubbles was not observed, concentrations of dissolved methane were significantly elevated (up to six-times background values) in the water column at various locations above the fracture, and microbial mats that form in the presence of methane were observed at the seafloor. Seismic amplitude anomalies revealed a bright spot at a fault bend that may be the source of the water column methane. Sediment porewaters recovered in close proximity to the Hugin Fracture indicate the presence of fluids from two different shallow (<500m) sources: (i) a reduced fluid characterized by elevated methane concentrations and/or high levels of dissolved sulfide (up to 6 mmol L^{-1}), and (ii) a low-chlorinity fluid (Cl ~305 mmol L^{-1}) that has low levels of dissolved methane and/or sulfide. The area of the seafloor affected by the presence of methane-enriched fluids is similar to the footprint of seepage from other morphological features in the North Sea.

1 Introduction

Methane-rich fluids are present worldwide in continental margin sediments (Judd and Hovland 2009) and sedimentary methane is a potential hazard that can trigger slope instabilities (Vanneste et al., 2014) and cause accidental blow-outs during hydrocarbon exploration drilling. Any methane that reaches the atmosphere will also act as a potent greenhouse gas, accelerating global warming (McGinnis et al., 2006, Skarke et al., 2015). It is estimated that geological sources, including marine methane release, contribute ~45 Tg yr^{-1} of methane to the atmosphere (Etiope et al. 2008; Kvenvolden and Rogers, 2005), which is <10% of global methane atmospheric emissions (Ciais et al., 2014). Recent estimates based on long-term carbon isotope records indicate that methane emission from natural gas, oil and coal production might, however, be much higher than previously suggested (Schwietzke et al., 2016). The importance of the marine contribution to methane emissions is uncertain as monitoring of fluid flow activity remains a challenge and uncertainties exist in understanding of fluid migration pathways, fluid alteration processes and leakage rates. Moreover, new seafloor features with methane-rich fluids in the near-surface sediments are continually being discovered (e.g. Krämer et al., 2017).

There are a number of reliable indicators for the presence of fluid flow activity and methane-rich fluids in near-surface sediments. These include geomorphological indicators such as the presence of pockmarks and mud volcanoes (Chen et al., 2015; Dupré et al., 2014; Holvand and Sommerville, 1985; Pierre et al., 2014) that are interpreted to be caused by sustained gas seepage from deeper hydrocarbon reservoirs that are in hydraulic connection with the sediment overburden (Karstens and Berndt, 2015; Nicoll et al., 2012; Heggland, 1997). These gases and fluids migrate from depth through buried faults and glacially-derived tunnel valleys that can reach the seabed and transfer material into the water column and ultimately to the atmosphere (Cartwright, 2011; Cartwright, 1994; Cavanagh and Haszeldine, 2014; Nicoll, 2012; Schroot et al., 2005; Wiprut and Zoback, 2000). The presence of fluid flow within shallow sediments can also be inferred from seismic reflection data by the presence of characteristic variations in the amplitude/reflection coefficient of the seismic signal (Cevatoglu et al., 2015; Tóth et al., 2014; Wiggins et al., 2015), and from steep gradients in porewater chemistry (e.g. Holvand et al., 2012). The chemical composition of the porewaters is strongly dependent on their origin, their migration and, as they are often highly reactive, their chemical transformation during transport. Finally, the presence of white microbial mats at the seafloor formed by giant filamentous sulfide oxidizing bacteria is often used as a proxy for the presence of reduced, methane-containing

fluids in the shallow subsurface (e.g. Hovland and Svensen, 2006; Hovland et al. 2012). These microbial mats live on the sulfide produced by the microbial turnover of methane with sulfate deeper in the sediment (anaerobic oxidation of methane: $CH_4 + SO_4^{2-} \rightarrow HS^- + HCO_3^- + H_2O$, (Eq. 1), Boetius et al. 2000) and can be detected by video-imaging and biogeochemical analyses of sediments. Methane oxidation can also be associated with the precipitation of methane-derived authigenic carbonates that accumulate at the seafloor or in the sediments (Aloisi et al., 2002). However, the presence of authigenic carbonates and specific chemosynthetic habitats largely depends on the rate of the fluid flow and they are not always visible at the sediment surface (Lichtschlag et al., 2010). If fluid flow rates are low or are variable with time (Grünke et al., 2011), near-surface seabed fluid flow can be hard to detect, but the fluids can still be an important source of reduced substances into surface sediments and a threat to drilling operations (e.g., Judd and Hovland, 2009). At high flow rates, the microbial filter that consumes methane within the sediments is not always effective. Thus release of methane to the water column is common, especially in shallow continental margins such as the North Sea, where the water column is frequently mixed by storms and methane emissions from the seabed can reach the atmosphere (Sommer et al., 2015; von Deimling et al., 2011).

The Central North Sea is a globally important hydrocarbon province. Numerous fluid flow structures exist in the shallow sediment overburden, including bright spots and seismic chimneys. Surface expressions of the presence of near-surface fluid flow activity include pockmarks and macro-seeps, such as the Tommeliten, the Scanner pockmark and the Gullfaks seep areas in the North Sea (Hovland et al., 2012). A new structure (Figure 1), the 3-km long Hugin Fracture, was discovered in 2011 in the Southern Viking Graben (Central North Sea, Norwegian Sector, block 16/4) and analysis of sub-bottom profiler data revealed the presence of bright spots that are interpreted to represent gas accumulations within the shallow strata (Landschulze and Pedersen, 2013; Landschulze et al., 2014; Pedersen et al., 2013). To determine the chemical composition and sources of material to the shallow sub-surface sediments, we conducted a multidisciplinary study of the shallow sediments in the vicinity of the Hugin Fracture. Fluid flow activity was monitored using geophysical tools mounted on an Autonomous Underwater Vehicle (AUV), shipboard multibeam bathymetry surveys and seabed video photography with a towed underwater vehicle. The composition of porewaters in the shallow subsurface sediments was verified by geochemical analyses of sediment cores. These data

indicate that the Hugin Fracture acts as conduit for fluid exchange between the subsurface sediments and the seafloor, and provides a source of methane to the overlying water column.

2 Geological setting and study area

The Hugin Fracture is located in the Southern Viking Graben (Utsira High) in the Central North Sea (Figure 1a). The Southern Viking Graben contains hydrocarbon-rich Paleocene sediments (Heimdal Formation) that are charged by Jurassic source rocks (Justwan and Dahl, 2005). The hydrocarbon-bearing units are overlain by the Miocene-Pliocene Utsira Formation. The uppermost Quaternary sediments are significantly disturbed by Pleistocene glaciations that led to episodic erosion and infill of the basin, with the formation of glacio-morphological features, including subglacial tunnel valleys and ploughmarks (Sejrup et al., 2000; Lonergan et al., 2006; Dowdeswell and Ottesen, 2013; Praeg, 2003).

Since 1996 the Utsira Formation has been used to store CO_2 that is a natural by-product of the gas extraction at the nearby Sleipner production site. The depth of the top of the Utsira Formation differs regionally from 550-1500 m below seafloor (Chadwick et al., 2004). The Utsira Formation is capped by the low permeability sands and mudstones of the Nordland Shales (Northland Group), which are assumed to act as effective seal for fluid migration from below (Harrington et al., 2009). Above that seal, shallow gas pockets can be present in the Northland Group sediments and seismic chimneys imply hydraulic connectivity between the strata (Karstens and Berndt, 2015).

3   Methods

A multidisciplinary study of the Hugin Fracture was carried out in 2012 during RRS *James Cook* cruise JC77. The main target areas for the study were the Hugin Fracture and its surrounding area, mainly south and east of the Hugin Fracture, but also including the abandoned hydrocarbon exploration well 16/4-2 (Figure 1). Detailed information on all sampling stations in the working area is given in Table S1.

3.1   Visual seafloor observations

High-quality visual imagery of the seabed was acquired with a 5 Mega-pixel digital downward looking color camera mounted on the AUV "Autosub 6000" with 60,000-70,000 image frames collected per deployment. More targeted observations were carried out with

HyBIS, a survey and sampling robotic underwater vehicle. The navigation of HyBIS was provided using the ship's Sonardyne USBL tracking system with a mini-transponder beacon on the HyBIS vehicle.

3.2   High-resolution 2D seismic reflection

High-resolution 2D seismic reflection data (Chirp) were acquired using an Edgetech 2200-M Modular Sonar System, mounted on the AUV. The source sweep used during seismic data acquisition was a high frequency Chirp sweep, developed by Gutowski et al. (2002) that oscillated between 2-13 kHz for 32 ms, with sine squared 8th envelope. The Chirp data were sampled at 43.4 kHz. The maximum penetration depth into the sediment was around 5 m (for V_p=1500 m/s) throughout the surveys. Due to the high quality of the collected data, only simple Chirp data processing was necessary: Correlation of the raw data with the source sweep, Ormsby band-pass filtering (1000-2000-10000-12000 Hz), minimum phase predictive deconvolution, trace mixing (3 traces), true amplitude recovery, trace muting, and instantaneous amplitude correction (Quinn et al., 1998; Cevatoglu et al., 2015). The processed Chirp data were then corrected for depth using the shipboard multibeam bathymetry data (EM710).

Root Mean Square (RMS) seismic amplitudes (A_{RMS}) were calculated for Chirp seismic reflection data using Eq. 2:

$$A_{RMS} = \sqrt{\frac{A_1^2 + A_2^2 + \cdots + A_m^2}{m}} \quad (Eq.2)$$

where *m* is the total number of samples within the selected time window. After the extraction of RMS seismic amplitude along trace, these values were gridded and RMS seismic amplitude maps produced. The limited electrical power available to drive the single transducer on the AUV, together with the coarse grain-size of the near-surface sediments, meant that the Chirp signal only penetrated the top 5 m of the sediment.

Side-scan sonar data were acquired with an Edgetech 2200-M Modular Sonar mounted on the AUV. The side-scan sonar operated at 410 kHz, with one-way beam being 0.3°, and 200 m swath. Survey speed was about 2.8 knots and the ping rate was approximately 0.3 m.

Following each AUV deployment, amplitude corrections were applied to the raw data, followed by the production of side-scan mosaics. The side-scan mosaics were processed at 0.5 m.

3.3 Geochemistry

3.3.1 Water column sampling and analyses

Water column methane concentrations were determined in water samples collected in Niskin bottles attached to a Conductivity, Temperature, Depth (CTD) rosette. A total of 63 CTD hydrocast transects were performed in the study area and samples for CH_4 analysis were collected at ~6, 8, 13 and 20 m above the seafloor and at 5 m below the seawater-air interface during each CTD deployment. To avoid contact with the atmosphere and the formation of bubbles, the seawater was collected in 500 mL blood bags using silicon tubing. Extraction of the methane from the seawater was done using the headspace method of Swinnerton et al. (1976); 60 mL of nitrogen headspace was introduced to all blood bags and the bags were allowed to equilibrate at 24°C for at least 2 hours. Methane concentration was determined by gas chromatography with flame ionization detector (GC-FID); to this end 20 mL of headspace gas was injected through a short desiccating column into the GC-FID and methane concentrations were determined from the area of peaks consistently produced at a retention time of 1.68 minutes. Peak heights were calibrated using 3 standards (a blank of pure N_2, 10 ppm CH_4 and 20 ppm CH_4) and an atmospheric measurement. Every 10 samples the 10 ppm CH_4 standard was re-run to check for instrument drift. The accuracy and precision of this technique is better than ±1%.

3.3.2 Sediment coring and geochemical analyses of porewaters and sediments

Sediment cores of up to 3.8 m length were collected using a vibrocorer at 12 stations at the Hugin Fracture, the abandoned well 16/4-2 and in the surrounding area (Table S1), at water depths between 83 to 99 m. Positions for sediment cores were selected with the help of HyBIS and AUV images. Comparison of the actual core length with the core penetration depth recorded by an echosounder mounted on the vibrocorer showed that loss of surface sediments during core recovery was minimal.

Immediately after retrieval, the vibrocores (VCs) were sectioned into 0.5 m intervals, capped and transported into a controlled temperature room cooled to in situ temperature (~7° C). Here, holes for sub-sampling were drilled into the plastic liners and taped to limit oxygen

contamination. For sub-sampling sediments and porewaters under an oxygen-free atmosphere the sections were transferred into an anaerobic chamber filled with nitrogen.

Porewater was extracted from sediments directly with Rhizons (Rhizon CSS: length 5 cm, pore diameter 0.2 μm; Rhizosphere Research Products, Wageningen, Netherlands) inserted through the pre-drilled holes in the VC liners and connected to a syringe to which a small under pressure was applied. For some of the dry sandy sediments outside the Hugin Fracture, sediment samples were removed using plastic syringes through larger holes in the VC liners, transferred into centrifuge vials inside the nitrogen-filled anaerobic chamber and centrifuged for 6-10 minutes at 10,000 rpm for compaction of the sediments. Afterwards, porewater was extracted from these sediments inside the anaerobic chamber with Rhizons inserted into the vials prior to centrifugation.

Aliquots of 2 mL of porewater were taken for dissolved inorganic carbon (DIC) analyses and for analysis of the carbon isotopic composition of the DIC ($\delta^{13}C_{DIC}$) and poisoned with mercuric chloride (5 μL) to prevent continued microbial turnover. A further 2.5 mL of the porewaters were acidified with 6 μL of concentrated suprapure HNO_3 for analyses of cations. 1-2 mL of the porewater were sub-sampled in the anaerobic chamber and fixed with zinc acetate for H_2S analyses and sub-samples were also taken for analysis of sulfate and chloride; these samples were also fixed with zinc acetate if sulfide was present. Total Alkalinity (TA) was measured on board immediately after porewater sampling, by titration against 0.0005 mol L^{-1} HCl using a mixture of methyl red and methylene blue as an indicator. Analyses were calibrated against IAPSO seawater (certified by the International Association for the Physical Sciences of the Oceans) and the reproducibility of the analyses was better than ±1%. Any remaining porewater was frozen at -20 °C for nutrient analyses.

To determine the methane concentration in the sediments 3 cm^3 of sediment was sampled using a cut-off syringe, transferred to a headspace vial containing 5 mL of 1 mol L^{-1} NaOH and crimp-sealed. Methane concentration was determined on board on 10 mL of the headspace by gas chromatography as described above. To determine the porosity of the sediment 5 cm^3 sub-samples were taken and stored in plastic containers at 4 °C. The porosity of the sediments was determined by the mass difference between wet and dried samples.

Back onshore, cation (B, Ba, Ca, Fe, Na, Li, Mg, Sr, Rb) concentrations were measured by inductively coupled plasma optical emission spectrometry (ICP-OES; Perkin-Elmer Optima 4300 DV) after diluting the samples by a factor of 50 with 3% thermally distilled HNO_3. Standards were prepared from single element standard solutions that covered the range of sample concentrations. Measured concentrations of a certified reference material seawater standard (CRM-SW; High Purity Standards) were within ±5% of the certified values for all elements. Anions were measured by ion chromatography (Dionex ICS 2500) with 9 mmol L^{-1} $NaCO_3$ as the eluent. Repeat analysis of IAPSO seawater and of single anion standards indicates that the reproducibility of the Cl and SO_4 analyses was better than ±1%. DIC was measured using an Apollo SciTech DIC analyzer (AS-C3), using a LI-COR CO_2/H_2O (LI-7000) infrared analyzer to detect CO_2 released from the sample after acidifying with 10% H_3PO_4. The carbon isotopic composition of the DIC ($\delta^{13}C_{DIC}$) was determined using a multiflow preparation system coupled to an Isoprime continuous flow mass spectrometer at Royal Holloway University of London. Measurements were made by injecting 0.5 mL of water into vials containing orthophosphoric acid that had been flushed with helium and equilibrating the acid and water for 4 hours at 40 °C (Mattey et al., 2008). $\delta^{13}C_{DIC}$ values were normalized to the VPDB (Vienna Pee Dee Belemnite) scale via a calibrated sodium bicarbonate internal standard and the standard deviation of 2 replicate measurements was less than ±0.3‰. Total dissolved sulphide concentrations (H_2S + HS^- + S^{2-}) were determined using the diamine method (Cline, 1969). Nutrient concentrations (phosphate, silicate, NOx, ammonium) were measured with a QuAAtro nutrient analyzer. $^{87}Sr/^{86}Sr$ isotope ratios in the porewaters were determined by thermal ionization mass spectrometry (TIMS). For the Sr isotope analysis a sub-sample of the porewater containing approximately 1 μg of Sr was loaded onto a column containing 50 μL of Sr-Spec resin. The sample matrix was eluted with 3 mol L^{-1} HNO_3, and the Sr fraction was then collected in MilliQ water. The purified Sr sample was dried and loaded onto a single Ta filament using a Ta activator solution and $^{87}Sr/^{86}Sr$ ratios were measured with a Thermo Fisher Triton Plus TIMS using a static routine with amplifier rotation with a ^{88}Sr beam intensity of 2V for 300 ratios. Results were normalized to a $^{86}Sr/^{88}Sr$ ratio of 0.1194 using an exponential correction. Analyses of the Sr isotope standard NBS987 give $^{87}Sr/^{86}Sr$ = 0.710247 ±0.000024 (2 SD; n = 106). The standard error of duplicate measurement was less than 17 ppm.

Sediment cores were split at the British Ocean Sediment Core Research Facility (BOSCORF) in Southampton, UK, and the archive half of each core was logged for magnetic

susceptibility with a XYZ Multi-Sensor Core Logger (Geotek) at 1 cm intervals. Relative abundances of elements were measured on the archive core half by X-ray fluorescence (ITRAX core-scanning X-ray fluorescence system, Cox Analytical; Croudace et al. 2006). The instrument was operated at a voltage of 30 kV and a current of 50 mA, with a count time of 30 s and at 1000 μm sample resolution. Element abundances are normalized to kcps (kilo-counts per second) and a running average of 0.5 cm was applied to the results.

3.3.3 Formation water sampling

Formation waters were sampled from the Ustira Formation. Samples were taken at wellbore 15/9-F-07 (58° 26' 29.87" N, 1° 53' 14.86" E, water depth 91 m) and 15/9-F-09 (58° 26' 29.74" N, 1° 53' 15" E, water depth 91 m) in 2011 and 2014. The wellbore penetrates the Utsira sands between ~880 – 1065 m below seafloor. pH and temperature were measured immediately after fluid recovery and the chemical composition of the fluids was determined in the same way as the porewater samples.

4 Results
4.1 Side scan, multibeam and seafloor observations

Side-scan sonar and optical imagery, together with sediment samples show that the seabed around the Hugin Fracture comprises sandy sediments, corresponding to low side-scan backscatter regions, and shell hashes that have higher backscatter (Figures 1, 2). The surface trace of the Hugin Fracture imaged on a side-scan sonar mosaic is around 1.6 km long, up to 5 m wide, has a very complex surface geometry (Figure 1 b-d), and appears as a sharp discontinuity on the seabed. The side-scan imagery reveals that the Hugin Fracture is made of two major fault segments, A and B, which are orientated NE-SW in an en echelon configuration, separated by a fault bend orientated NW-SE. The more easterly fault segment, Segment A, comprises zig-zagging, sub-parallel fractures, oriented NE-SW, and imaged over approximately 260 m (Figure 1d). These subsidiary fractures are connected to each other via small fault bends in a NW-SE direction. Segment B is around 1.2 km long and fairly linear, oriented NE-SW; however smaller fault bends and step overs oriented NW-SE are also found along strike, connecting zig-zagging more minor fractures. Unlike Segment A, Segment B is more discontinuous towards its end, suggesting burial by mobile surficial sediments (Figure 1d). In places (for example at the western end of Segment B), splaying of the fault segment is seen with two surface traces. Although the fault traces look relatively fresh, there is little change in depth along or across the

Hugin Fracture (varying between 93-94 m depth), although north of the main fault bend the seabed is slightly depressed.

Black sediments, with and without white mats formed by sulfide oxidizing bacteria, are evidence for the presence of methane-rich fluids in the near-surface sediments along the Hugin Fracture and in the vicinity of abandoned well 16/4-2 (Figure 2). At well 16/4-2, video images collected using the HyBIS remotely operated vehicle show bubbles venting from the sediment into the water column, and large patches with microbial mats cover the sediment. Evidence for the presence of reduced, methane-enriched fluids in near-surface sediments all along the Hugin Fracture is provided by the continuous presence of microbial mats and dark sediment patches. However, no seabed authigenic carbonates or bubble streams were detected along the fracture during our survey. Black spots and microbial mats extend about 10 m perpendicular to the fracture. Apart from along the Hugin Fracture and at well 16/4-2, there is no other visual evidence of fluid flow activity or bubble plumes within our 25 km^2 survey area.

4.2. Seismic Reflection Amplitude Mapping

On Chirp seismic reflection data, the Hugin Fracture appears as a sharp, sub-vertical discontinuity, traced down to approximately 5 m below the seabed (Figure 3), and is associated with sub-meter scale vertical displacement. Further analysis of Chirp data reveals high amplitude seismic reflection anomalies within the overburden, along the Hugin Fracture and at the abandoned well 16/4-2, concentrated at around 1 m depth below the seabed. However, gas flares are only observed at the abandoned well site from Chirp data, consistent with overburden seismic anomalies detected at this location, whereas no indication of fluid venting at the seafloor is found at the Hugin Fracture from the Chirp dataset.

A Root Mean Square (RMS) seismic amplitude map, superimposed on the side-scan data, illustrates seismic amplitudes to ca. 2.5 m below the seabed from the Chirp data (Figure 4). The eastern side of the Hugin Fracture area, including the Hugin Fracture, has been found to have slightly higher seismic amplitudes compared to the western side of the survey area. The largest seismic amplitude anomalies are restricted to the main fault bend along the Hugin Fracture and to the abandoned well site. These very localized seismic amplitude anomalies, especially along the Hugin Fracture, likely indicate a patchy fluid flow pattern along this seabed discontinuity, rather than a continuous fluid flow activity throughout the fracture (Figure 2).

4.3. Geochemistry

4.3.1 Methane distribution in the water column

Figure 5 shows the distribution of dissolved methane in the water column within the study area. Within 20 m of the seabed of the area to the south of the Hugin Fracture, methane concentrations range between 30 and 930 nmol L^{-1} with an average of 310 ±250 (average ±SD) nmol L^{-1} (Figure 5a). Methane concentrations in the area around the abandoned well, which has a methane release rate of ~4 t CH_4 yr^{-1} (Vielstädte et al., 2015), are 660 ±140 nmol L^{-1} (Figure 5b). In the vicinity of the Hugin Fracture methane concentrations are between 1050 and 3160 nmol L^{-1} with an average of 1950 ±620 nmol L^{-1} (Figure 5b). This value is far higher than that measured in bottom waters to the south of the Hugin Fracture, and values measured in the vicinity of the abandoned well (which is >2 km from the Hugin Fracture). Although highest methane concentrations are found above Segment A of the Hugin Fracture, high methane concentrations also occur above Segment B at several locations (Figure 5b). In the surface waters methane concentrations are ~20 ±10 nmol L^{-1}.

4.3.2 Sediment lithology and geochemistry

Locations of sediment cores taken at the Hugin Fracture are given in Figure 4. The upper 3.8 m of the subseabed sediments recovered with the VCs is characterized by three different horizons (Figures 6, S1, S2): (i) a surface layer that usually has a thickness of 5-25 cm and consists of sandy sediments of dark brown colour; (ii) a shelly layer of up to 5-15 cm thickness, which is present in most of the cores; and (iii) a lower layer of sandy sediments that have a uniform appearance. The upper 2 layers are characterized by high Fe and S concentrations that correlate with increases in magnetic susceptibility. High magnetic susceptibility indicates the presence of magnetic Fe-S minerals (Figure 6). These uppermost sediments also show intervals with high Ca concentrations that coincide with the occurrence of bivalve shell debris. The chemical composition of sediments in the lowermost sandy layer is relatively uniform, except for occasional increases in Ca, Fe and S content (e.g. in VC10; Figure 6b) that coincide with the presence of single shells. The porosity of the sediments is 0.37 ±0.03 and is relatively constant both within cores and between cores. No authigenic carbonates were found in the upper 3.8 m of the sediments or at the sediment surface.

4.3.2 Porewater geochemistry

Results of sediment porewater analyses of anions, cations, methane, sulfide, nutrients, DIC, TA and $\delta^{13}C_{DIC}$ are shown in Figure 6. Dissolved sulfide in porewaters was detected in all four cores sampled close to the Hugin Fracture (VC08, VC10, VC14, VC28; Figure 6a-e). Highest concentrations of dissolved sulfide are found in cores VC08 and VC10 (eastern part of Segment B, up to 6.0 mmol L^{-1} and 4.5 mmol L^{-1}, respectively) and lower concentrations were measured in VC14 (up to 0.3 mmol L^{-1}) and VC28, (up to 1.4 mmol L^{-1}). Note that concentrations of dissolved sulfide are very low at the top, and bottom, of these two cores. Low concentrations of dissolved sulfide coincide with increases in solid phase S and Fe and magnetic susceptibility, indicating sulfide removal by iron-sulfide precipitation. In cores sampled further from the Hugin Fracture, sulfide concentrations are below detection limit.

Methane concentrations are elevated in the upper 0.5 m of one core (VC08) with concentrations reaching ~800 μmol L^{-1} at 0.2 m (Figure 6a). In all other cores containing sulfide, methane concentrations are 2 orders of magnitude lower (<6 μmol L^{-1}, Figure 6a-e). The measured maximum methane concentration is lower than atmospheric saturation (~1.6 mmol L^{-1} at 7 ºC; Yamamoto et al., 1976), which is consistent with the lack of gas bubbles observed in the vicinity of the Hugin Fracture, and there were no visual signs of degassing of sediments upon recovery. In cores with negligible sulfide, methane concentrations are <0.5 μmol L^{-1} (Figure 6d, Figure S1).

Concentrations of sulfate, which is the electron acceptor for anaerobic oxidation of methane, are lowest in cores that have highest sulfide concentrations (Figure 6a-e). In VC08, between 0.2 and 0.5 m sediment depth, sulfate is <1 mmol L^{-1} (Figure 6a) and methane was detected in this sediment interval. Sulfate concentrations increase again below the methane-rich zone reaching ~15 mmol L^{-1} below 2.5 m. This value is about 50% lower than in cores where no sulfide was found in the porewater. In core VC10, concentrations of sulfate are rather constant throughout the core (4-11 mmol L^{-1}, Figure 6b) and sulfide concentrations remain high. In VC14, where sulfide concentrations are only slightly above background, sulfate concentrations (10-15 mmol L^{-1}, Figure 6c) are ~50% lower than in cores without sulfide.

Most sediment porewaters have TA concentrations of 2.6 ±0.3 mmol L^{-1} and DIC concentrations of 2.6 ±0.1 mmol L^{-1}. However, much higher TA and DIC concentrations (19.5 and 13.0 mmol L^{-1}, respectively) are found in the upper 1.4 m of VC08, although they decrease to ~7.5 mmol L^{-1} (TA) and 6 mmol L^{-1} (DIC) below 2 m. In VC10 TA and DIC concentrations are also elevated, but are relatively constant (6-10 mmol L^{-1}) throughout the core. Both VC14 and VC28 have clearly elevated DIC and TA concentrations. Core VC23, from the abandoned

well 16/4-2, also has slightly elevated TA (3.5 mmol L^{-1}) and DIC (5 mmol L^{-1}), but no increase of sulfide or decrease of sulfate is detected.

The δ^{13}C signatures of the porewater DIC range from -57‰ to 0‰ VPDB. Lowest δ^{13}C$_{DIC}$ values are found in porewaters with high sulfide and high methane (VC08, 0.8 m). Low δ^{13}C$_{DIC}$ values (~-50‰ VPDB) are also found in VC10. In the two other cores in which sulfide was detected, δ^{13}C$_{DIC}$ values are slightly less negative and range from -20 to -35‰ VPDB in VC14 and from -12 to -40‰ VPDB in VC28. The δ^{13}C$_{DIC}$ value of porewaters in sediments close to the abandoned well 16/4-2 (VC23) is ~-5‰. In all other cores δ^{13}C$_{DIC}$ signatures range between -3 ±2‰ VPDB. In summary, all cores collected close to the Hugin Fracture (VC08, VC10, VC14, VC28) show the presence of reduced fluids, i.e. high sulfide, TA and DIC concentrations, low sulfate concentrations and a negative δ^{13}C$_{DIC}$ signature. In contrast, cores collected further away from the Hugin Fracture (e.g. VC04, Fig 6e) have seawater sulfate concentrations and δ^{13}C$_{DIC}$ signatures and low sulfide and methane concentrations. Site VC04 is subsequently referred to as the 'background' site; other background sites are not discussed in detail, but data from them are shown in Figure S1.

In cores that show the presence of reduced fluids, chloride concentrations are around 305 mmol L^{-1} ±16 mmol L^{-1} below 0.5 m (Figure 6a-e), which is lower than the chloride concentration in the porewaters at the background sites (540 ±65 mmol L^{-1}). In the same cores, concentrations of porewater Si and Ba are enriched up to 3-times (Si) and up to 40-times (Ba) compared to background sites (Figure 6, Table 1). Dissolved ammonium is also 10-fold higher in these cores (Figure 6). In contrast, other elements are depleted in the reduced fluids compared to background concentrations, such as Li (0.6-times background), Sr (0.7-times background), Ca (0.7-times background) and Mg (0.6-times background) (Figure 6). Concentrations of Fe only slightly increased with depth at the background sites (Figure 6d), and were generally low in the cores with reduced fluids (mostly <1 µmol L^{-1}, Figure 6a-d).

The Sr isotopic composition of porewaters from the background site VC04 is ~0.70915 to 0.70916, close to modern seawater (0.70918, Mokadem et al., 2015). Porewaters from sites close to the Hugin Fracture tend to have slightly more radiogenic ^{87}Sr/^{86}Sr values, ranging from 0.70917 to 0.70928 (Figure 7, Table S2), with highest values measured in VC10. In VC08, ^{87}Sr/^{86}Sr values are similar to VC10 in porewaters with highest sulfide concentrations, but they are close to background site values below 2.6 m sediment depth.

4.3.4 Composition of Utsira Formation waters

Results of the analyses of the Utsira Formation waters are displayed in Table 1 together with the compositions of background sediment porewaters and the reduced fluids sampled close to the Hugin Fracture. Most notably, the Utsira Formation waters contain an order of magnitude more Li and B relative to the background porewaters. Concentrations of Mg and Ca are slightly lower than the background porewaters (0.4-0.8 times), and the formation waters have very low sulfate concentrations (<0.5 mmol L^{-1}), but sulfide concentrations are below detection limit. In contrast to many formation waters, Utsira Formation waters are not particularly saline, and their Na-Cl content is close to that of seawater. The Sr isotopic composition ($^{87}Sr/^{86}Sr$) of Utsira Formation water is 0.70924 (Figure 7), which is more radiogenic than modern-day seawater (0.70918, Mokadem et al., 2015).

5 Discussion

5.1 Hugin Fracture fluid composition and origin

Our geochemical and geophysical analyses indicate that the Hugin Fracture is a site of increased fluid flow activity and that reduced fluids are present in the near-surface sediments along the fracture. The chemical composition of the porewaters can be used to assess the origin of the fluids and to determine the extent to which their chemistry is modified by diagenetic and biogeochemical processes occurring in the shallow subsurface.

5.1.2 Fluid origin

The connectivity of the Hugin Fracture with the strata below the Northland Shales, i.e. below 550 m below the seafloor, can be assessed by comparison between the geochemical composition of Utsira Formation fluids and porewaters in the shallow subsurface sediments (Table 1). The Cl concentration of sediment porewaters in the vicinity of the Hugin Fracture is ~50% lower than it is in the Utsira Formation fluids (~305 vs. ~540 mmol L^{-1}), and the porewaters have far lower concentrations of Li and B. High levels of Li and B in the formation fluids are likely due to reaction of the formation water with the reservoir sands: dissolution of B and Li from silicate minerals occurs at moderate temperatures (50-350 °C; e.g. James et al., 2003; Wimpenny et al., 2010). Rb is not usually leached at these temperature (James et al., 2003), which is also consistent with our observations. The $^{87}Sr/^{86}Sr$ ratio of the formation water

is higher than that expected of Miocene-Pliocene-aged seawater (McArthur et al., 2001), which is also consistent with input of radiogenic Sr from the reservoir sands. We conclude that Li and B are likely to be effective tracers of Utsira Formation water, as they are enriched by an order of magnitude compared to background porewaters, and are in general relatively unreactive during transport through the overlying sediment column. However, as concentrations of both elements are similar to seawater in the porewaters sampled along the Hugin Fracture (Table 1), we conclude that Utsira Formation fluids are unlikely to be a source to the Hugin Fracture. Rather, fluids circulating within shallow subsurface sediments along the fracture must originate from within sediments located above the impermeable Northland Shale seal, i.e. < 550 m below the seafloor.

A shallow fluid source is also suggested by the carbon isotopic composition of the DIC. The carbon isotopic composition of methane ($\delta^{13}C_{CH4}$) in surface sediments sampled during another expedition to the Hugin Fracture is between -85 and -32‰ VPDB, which indicates a microbial source (Haeckel et al., 2013). The $\delta^{13}C_{CH4}$ value of methane discharged from abandoned well 16/4-2 (-70‰ VPDB; Vielstädte et al., 2015) is within this range. Given that methane from deep hydrocarbon reservoirs in the North Sea has a much higher (thermogenic) $\delta^{13}C_{CH4}$ value (~-40‰ VPDB, James, 1990), and based on the thermal gradient in this area, the microbial methane must be produced <2 km below the seafloor (Vielstädte et al., 2015). Hydrogen carbonate ions produced by anaerobic oxidation of methane (Eq. 1) contribute to the DIC content of sediment porewaters, and will have a carbon isotope signature that reflects that of the methane from which it forms (Reeburgh, 2007). Our $\delta^{13}C_{DIC}$ analyses show that porewaters from intervals with high sulfide concentrations have very low $\delta^{13}C_{DIC}$ values (~-57‰ VPDB) compared to background values of 0‰ VPDB (Figure 6a). This strongly suggests that the methane has a biogenic source. Shallow pockets of gas have been described in the Pliocene-Pleistocene sediments above the Utsira Formation and may well be the source of the methane in the shallow subsurface sediments (Karstens and Berndt, 2015, Vielstädte et al., 2015).

Further evidence that the source of the near-surface fluids in the Hugin Fracture lies within younger sediments above the Northland Shale comes from their Cl concentrations; porewaters from the Hugin Fracture have lower Cl concentrations compared to porewaters from outside the fracture. Cl behaves conservatively in the marine environment, so the presence of low Cl concentrations indicates that the porewaters in the Hugin Fracture have a different

14 | P a g e

source. Low-Cl fluids can be produced by dissolution of methane hydrates or ingression of freshwater. Methane hydrate is unstable at the temperature and pressure conditions within the shallow subsurface sediments in this area, but this area was likely covered by ice during some parts of the last glacial period (e.g. Boulton & Hagedorn, 2006), so the sediments could contain a freshwater component. The oxygen and deuterium isotopic compositions of porewaters from within 10 cm of the seafloor also indicate the presence of meteoric water (Haeckel et al., 2013).

5.2. Biogeochemical and diagenetic processes

Black sediment patches and white microbial mats along the Hugin Fracture indicate the presence of methane in the shallow subsurface sediments (Judd and Hovland, 2009) and anaerobic oxidation of methane with sulfate close to the seafloor (Boetius et al., 2000). Anaerobic oxidation of methane explains the low levels of methane and sulfate (VC08, Figure 6a) and the high concentrations of ^{13}C–depleted DIC and sulfide in all porewaters close to the Hugin Fracture. In organic carbon-rich sediments, low concentrations of porewater sulfate and high concentrations of porewater sulfide can be associated with sulfate reduction coupled to anaerobic degradation of organic matter once other electron acceptors (oxygen, nitrate, Fe- and Mn-oxides) have been depleted. However, this process does not seem to be important in this part of the North Sea, as sulfide is not present in sediment porewaters outside the Hugin Fracture and the carbon isotopic composition of the DIC (-57 ‰ VPDB) indicates a microbial methane source (Reeburgh, 2007). Thus, although methane concentrations measured in our cores from the Hugin Fracture are relatively low, DIC data provide evidence for its microbial conversion in the shallow subsurface (Figure 6a).

Porewaters containing higher concentrations of sulfide (i.e. VC08, VC10; VC28; Figure 6) are also characterized by relatively low levels of Ca, which may indicate authigenic carbonate precipitation due to the production of HCO_3^- during anaerobic methane oxidation (Eq. 1, Aloisi et al., 2002; Luff and Wallmann, 2003). The increase of Ba in these fluids may be due to dissolution of barite ($BaSO_4$), which is a potential substrate for methane oxidation below the depth of sulfate depletion (Torres et al., 1996). However, there is no obvious loss of Ba from the solid phase in the uppermost sediments (data not shown) and no authigenic carbonates were found, so these reactions must have occurred elsewhere in the sedimentary overburden. These Ca-depleted, Ba-enriched fluids indicate that part of the methane may have been removed deeper in the sediments by anaerobic methane oxidation.

Oxidation of methane with sulfate usually results in a sharp transition from methane-rich sulfate-free porewaters to overlying methane-poor sulfate-rich porewaters (the 'sulfate-methane transition zone'; Borowski et al., 1996; Hensen et al., 2003). However, sulfate porewater concentrations at some sites along the Hugin Fracture increase again below this transition zone (Figure 6a), or sulfate has nearly constant concentrations in the upper part of the sediment column (Figure 6c). In the same cores, methane concentrations remain at background values (Figure 6a, c), except in VC08 where methane concentrations were <0.8 mmol L^{-1}. One explanation for this pattern is that the methane-rich and the low-salinity fluids have a different source. For example, in core VC14 (Figure 6c), concentrations of both sulfate and chloride are ~50% lower than in the background sites, which implies that sulfate removal by methane deeper in the sediment was not an important process. Sulfide re-oxidation could have occurred by an unknown process in the deeper sediments, but $\delta^{13}C_{DIC}$ values (-20‰ VPDB) are significantly higher than they are in the methane-rich intervals (-57‰ VPDB). At this site, concentrations of total alkalinity and DIC are clearly higher than at the background sites and are consistent with the effects of organic carbon diagenesis; this explanation is supported by higher than background concentrations of ammonium, which is released during the remineralization of organic carbon (e.g. Froehlich et al., 1979).

Hence we suggest that fluids circulating within the shallow subsurface sediments in the vicinity of the Hugin Fracture come from two different sources: (i) A fluid that contains methane that is mostly consumed by anaerobic methane oxidation, resulting in the higher concentrations of porewater sulfide, TA and δ^{13}C-depleted DIC. This fluid probably originates from shallow gas pockets in the Pliocene-Pleistocene sediments. (ii) A fluid that has low levels of methane and sulfide, low Cl, and slightly elevated levels of DIC and TA. This fluid may have entrained glacial melt water that formed when the study area was located closer to the coastline or was covered by ice. The presence of two different fluid sources is also supported by measurements of porewater Sr isotope compositions. All porewaters from close to the Hugin Fracture are enriched in radiogenic Sr compared to the background site, but fluids with low Cl tend to have higher ^{87}Sr/^{86}Sr (~0.7928) than fluids that Cl concentrations close to seawater (~0.7920) (Figure 7, Table S2). Fluids usually acquire radiogenic Sr isotope ratios during interactions with continental crust or terrigenous material (Elderfield & Gieskes, 1982).

Geophysical imaging confirms that there are hotspots of gas or gas-enriched fluids, most notably at the fault bend in the Hugin Fracture (Figures 3, 4). This fault bend thus potentially represents a hydraulic connection to the shallow gas pockets in the Pliocene-Pleistocene sediments above the Utsira Formation. We hypothesize that in the upper few meters of the sediment a connected fracture network exists that transports reduced methane-enriched fluids. Transport of these fluids likely occurs both horizontally as well as vertically, because the dissolved sulfide distribution indicates that methane is only present in the upper 1 m of the sediment in cores VC14 and VC28. Nevertheless there is evidence (i.e. higher sulfide, TA, DIC concentrations and low $\delta^{13}C_{DIC}$ values) for anaerobic oxidation of methane at deeper depths in core VC10. Horizontal transport of methane is facilitated by differences in the permeability and/or porosity of different sediment layers; for example, methane-consumption is only observed in distinct layers within subsurface sediments at the Tommeliten seep area (Niemann et al., 2005). In the Hugin Fracture area, horizontal gas migration may occur in the shelly layer.

5.2 Shallow fluid flow at the Hugin Fracture in a global context

The presence of methane- and sulfide-containing, reduced fluids in shallow sediments can have broad ecological and biological implications for the marine environment, providing chemosynthetic energy to usually energy-depleted parts of the ocean, but potentially also releasing a potent greenhouse gas into the water column and the atmosphere. In the Central and Northern North Sea, the presence of methane and its oxidation products in shallow subsurface sediments and methane release to the water column has been demonstrated at seabed pockmarks (Hovland et al., 2012) and at abandoned hydrocarbon exploration wells (e.g. Vielstädte et al., 2015). The discovery of reduced fluids and evidence for the presence of shallow methane (high sulfide concentrations, bacterial mats) in the Hugin Fracture sediments suggests that fractures may also be important fluid migration pathways in the North Sea. Fault-related methane seepage structures have mainly been observed in tectonically active areas such as the Marmara Sea (Dupre et al., 2015), the Santa Barbara Basin (Eichhubl et al., 2000) and the Nankai Trough (Henry et al., 2002). Our study shows that the Hugin Fracture is an active conduit transferring fluids from the deeper in the sediment column (<500 m below the seafloor) into surface sediments, with visual and geophysical indicators for near-surface fluid flow, biogeochemical turnover of methane and large spatial variabilities.

Above sites of focused methane discharge, such as the Håkon Mosby mud volcano (Sauter et al., 2006) and mud volcanoes in the Gulf of Cadiz (Sommer et al., 2009), methane concentrations can be >10,000 nmol L^{-1}. In the North Sea, background dissolved methane concentrations are typically ~ 5-10 nmol L^{-1} (von Deimling et al., 2011); concentrations as high as 400,000 nmol L^{-1} have been measured at North Sea blow-out sites (von Deimling et al., 2015). In the vicinity of the Hugin Fracture methane concentrations reach up to 3160 nmol L^{-1} (Figure 5), which indicates that part of the methane in the shallow sub-seabed sediments in the vicinity of the fracture is not consumed by the microbial filter in the sediments, but is transferred to the water column. The lack of gas flares in the water column close to the fracture suggests that the majority of the methane emitted from the sediments is probably in dissolved form as found at other seep locations (McGinnis et al., 2006, Sauer et al., 2015) or that methane emissions are ephemeral. Ephemeral gas emissions have been observed at the Marmara fault (Dupre et al., 2015).

From the lack of gas bubbles, the relatively low methane concentrations measured in the water column, and the evidence for anaerobic oxidation of methane in sediment porewaters, we conclude that the methane supply to the fracture is medium to low. If the methane flux is relatively low, then the sulfate flux from seawater into the sediment is high enough to consume most of the methane. At the Hugin Fracture the sediment porewaters are not completely sulfate depleted, and sulfide concentrations (0.3 - 6 mmol L^{-1}) are relatively low compared to other cold seeps (e.g. >12 mmol L^{-1} at Håkon Mosby Mud Volcano and the Amon Mud Volcano (Felden et al., 2013; Lichtschlag et al., 2010), ~20 mmol L^{-1} in the Gulf of Mexico (Aharon and Fu, 2000), ~6 mmol L^{-1} at the Tommeliten Field (Niemann et al.. 2005)).

The distribution of microbial mats along the Hugin Fracture is patchy, suggesting that the methane flux may also be spatially variable. Highest porewater sulfide concentrations are found at different depths at different sites (0.3-1 mbsf), and are variable (0.3 - 6 mmol L^{-1}). Trapping of methane below microbial mats can also result in heterogeneities in the methane distribution in sediments, as reported for other parts of the North Sea (Hovland, 2002). Nevertheless, if mats are visible, sulfide must be present close to the sediment surface so that the oxygen- and nitrate-dependent, sulfide oxidizing bacteria can thrive. The absence of microbial mats does not necessarily indicate the absence of sulfide production; if reactive iron-minerals are present in the sediments, dissolved sulfide can be immobilized in the form of iron-sulfide minerals and may

not reach the sediment surface (Fe-S solid phase peaks Figure 6a, b, d). Over time, this barrier may be overcome as the supply of reactive iron-minerals is depleted, allowing bacterial mats to form on top of the sediments. Taking into account the total length of the Hugin Fracture (3 km), and assuming that reduced fluids are found within 5-10 m either side of the fracture as suggested by the AUV imagery, the area of the Hugin Fracture that contains reduced, sulfide-rich fluids comprises up to 0.03-0.06 km^2 of the seafloor. This areal extent is likely to be a minimum estimate because, as discussed above, precipitation of sulfides may prevent the formation of bacterial mats at the seafloor. This area is slightly smaller than other known methane seeps area in the North Sea, such as the 'Heincke' site (0.1 km^2) and Tommeliten (0.12 km^3); however, active seepage only occurs over a fraction of their surface area (Hovland et al., 2012, Judd and Hovland, 2009) so the Hugin Fracture may be of similar importance as a chemosynthetic hotspot as other fluid flow structures in the North Sea.

5.3 Monitoring of fluid flow across the seabed

There is an increasing need to develop accurate and cost-effective monitoring technologies that can be reliably used to quantify the extent and flux of reduced, methane-rich fluids to shallow sediments. Although the Central North Sea is extremely well-surveyed, the Hugin Fracture was discovered only recently (Pedersen et al., 2013). Here, we show that the fracture hosts reduced fluids in the near-surface sediments and the areal extent of these fluids may be similar to that of much larger features such as pockmarks. By comparing the different geochemical and geophysical approaches that were applied in the survey of the Hugin Fracture, we have identified various effective monitoring strategies:

- AUVs may be used to locate and investigate fluid flow structures using geophysical and geochemical sensing instruments.

- Formation waters often have a different geochemical composition from the surface porewaters, and relatively unreactive chemical species such as Li or B can be used to trace the origin, depth and connectivity of deep reservoirs with the sediment overburden. Knowledge of the composition of formation fluids may be important for assessing the integrity of subseafloor CO_2 storage sites.

- The chemical composition of sediment porewaters allows different fluid sources to be distinguished.

- The absence of gas bubbles, microbial mats and sediment black spots does not necessarily indicate the absence of fluid transport into shallow subsurface sediments, as fluid flow can be variable in space and time. Porewater chemistry can reveal the presence of reduced fluids in the subsurface, even if there is no surface expression.

- Along the Hugin Fracture, methane anomalies in the water column have been detected using traditional sampling techniques from a ship, but these may not be suitable for detecting smaller point sources (such as the abandoned wells). Source localization at smaller scales requires more advanced methods, such as sensors mounted on AUVs.

Conflict of interest statement

The authors declare that the research was conducted in the absence of any commercial or financial relationships that could be construed as a potential conflict of interest.

References

Aharon, P. and Fu, B.: Microbial sulfate reduction rates and sulfur and oxygen isotope fractionations at oil and gas seeps in deepwater Gulf of Mexico, Geochimica et Cosmochimica Acta, 64, 233-246, 2000.

Aloisi, G., Bouloubassi, I., Heijs, S. K., Pancost, R. D., Pierre, C., Damsté, J. S. S., Gottschal, J. C., Forney, L. J., and Rouchy, J.-M.: CH_4-consuming microorganisms and the formation of carbonate crusts at cold seeps, Earth and Planetary Science Letters, 203, 195-203, 2002.

Boetius, A., Ravenschlag, K., Schubert, C. J., Rickert, D., Widdel, F., Gieseke, A., Amann, R., Jørgensen, B. B., Witte, U., and Pfannkuche, O.: A marine microbial consortium apparently mediating anaerobic oxidation of methane, Nature, 407, 623-626, 2000.

Borowski, W. S., Paull, C. K., and Ussler, W.: Marine pore-water sulfate profiles indicate in situ methane flux from underlying gas hydrate, Geology, 24, 655-658, 1996.

Boulton, G., & Hagdorn, M.: Glaciology of the British Isles Ice Sheet during the last glacial cycle: form, flow, streams and lobes. Quaternary Science Reviews, 25, 3359-3390, 2006.

Cartwright, J.: Diagenetically induced shear failure of fine-grained sediments and the development of polygonal fault systems, Marine and Petroleum Geology, 28, 1593-1610, 2011.

Cartwright, J. A.: Episodic basin-wide fluid expulsion from geopressured shale sequences in the North Sea basin, Geology, 22, 447-450, 1994.

Cavanagh, A. J. and Haszeldine, R. S.: The Sleipner storage site: Capillary flow modeling of a layered CO_2 plume requires fractured shale barriers within the Utsira Formation, International Journal of Greenhouse Gas Control, 21, 101-112, 2014.

Cevatoglu, M., Bull, J. M., Vardy, M. E., Gernon, T. M., Wright, I. C., and Long, D.: Gas migration pathways, controlling mechanisms and changes in sediment acoustic properties observed in a controlled sub-seabed CO_2 release experiment, International Journal of Greenhouse Gas Control, 38, 26-43, 2015.

Chadwick, R., Zweigel, P., Gregersen, U., Kirby, G., Holloway, S., and Johannessen, P.: Geological reservoir characterization of a CO_2 storage site: the Utsira Sand, Sleipner, northern North Sea, Energy, 29, 1371-1381, 2004.

Chen, J., Song, H., Guan, Y., Yang, S., Pinheiro, L. M., Bai, Y., Liu, B., and Geng, M.: Morphologies, classification and genesis of pockmarks, mud volcanoes and associated fluid escape features in the northern Zhongjiannan Basin, South China Sea, Deep Sea Research Part II: Topical Studies in Oceanography, 122, 106-117, 2015.

Ciais P., Sabine C., Bala G., Bopp L., Brovkin V., Canadell J., Chhabra A., DeFries R., Galloway J., Heimann M., Jones C.: Carbon and other biogeochemical cycles. In Climate change 2013: the physical science basis. Contribution of Working Group I to the Fifth Assessment Report of the Intergovernmental Panel on Climate Change 2014 Apr (pp. 465-570). Cambridge University Press, 2014.

Cline, J. D.: Spectrophotometric determination of hydrogen sulfide in natural waters, Limnol Oceanogr, 14, 454-&, 1969.

Croudace, I. W., Rindby, A., and Rothwell, R. G.: ITRAX: description and evaluation of a new multi-function X-ray core scanner, Special publication-geological society of London, 267, 51, 2006.

Dowdeswell, J. and Ottesen, D.: Buried iceberg ploughmarks in the early Quaternary sediments of the central North Sea: a two-million year record of glacial influence from 3D seismic data, Marine Geology, 344, 1-9, 2013.

Dupré, S., Mascle, J., Foucher, J.-P., Harmegnies, F., Woodside, J., and Pierre, C.: Warm brine lakes in craters of active mud volcanoes, Menes caldera off NW Egypt: evidence for deep-rooted thermogenic processes, Geo-Marine Letters, 34, 153-168, 2014.

Eichhubl, P., Greene, H., Naehr, T., and Maher, N.: Structural control of fluid flow: offshore fluid seepage in the Santa Barbara Basin, California, Journal of Geochemical Exploration, 69, 545-549, 2000.

Elderfield, H. and Gieskes, J. M.: Sr isotopes in interstitial waters of marine sediments from Deep Sea Drilling Project cores, Nature, 300, 493-497, 1982.

Etiope, G., Lassey, K. R., Klusman, R. W., and Boschi, E.: Reappraisal of the fossil methane budget and related emission from geologic sources, Geophysical Research Letters, 35, 2008.

Felden, J., Lichtschlag, A., Wenzhöfer, F., de Beer, D., Feseker, T., Pop Ristova, P., De Lange, G., and Boetius, A.: Limitations of microbial hydrocarbon degradation at the Amon mud volcano (Nile deep-sea fan), Biogeosciences, 10, 3269-3283, 2013.

Froelich, P., Klinkhammer, G. P., Bender, M. L., Luedtke, N. A., Heath, G. R., Cullen, D., ... & Maynard, V. Early oxidation of organic matter in pelagic sediments of the eastern equatorial Atlantic: suboxic diagenesis. Geochimica et Cosmochimica Acta, 43, 1075-1090, 1979.

Gutowski, M., Bull, J., Henstock, T., Dix, J., Hogarth, P., Leighton, T., and White, P.: Chirp sub-bottom profiler source signature design and field testing, Marine Geophysical Researches, 23, 481-492, 2002.

Grünke, S., Felden, J., Lichtschlag, A., Girnth, A. C., De Beer, D., Wenzhöfer, F., and Boetius, A.: Niche differentiation among mat-forming, sulfide-oxidizing bacteria at cold seeps of the Nile Deep Sea Fan (Eastern Mediterranean Sea), Geobiology, 9, 330-348, 2011.

Haeckel, M., Wallmann, K., Schmidt, M., Liebetrau, V., Sommer, S., Schroller, D., Schoenfeld, J., Karstens, J., and Berndt, C.: Fluid expulsion at a 3-km long fracture system in the Northern North Sea - geochemical constraints on the origin of gas and water, AGU Fall Meeting, San Fransisco, USA, 2013.

Harrington, J.F., Noy, D.J., Horseman, S.T., Birchall, D.J., Chadwick, R.A.: Laboratory study of gas and water flow in the Nordland Shale, Sleipner, North Sea. In: Carbon Dioxide Sequestration in Geological Media–State of the Science. In: AAPG Studies in Geology, vol.59, 2009

Henry, P., Lallemant, S., Nakamura, K.-i., Tsunogai, U., Mazzotti, S., and Kobayashi, K.: Surface expression of fluid venting at the toe of the Nankai wedge and implications for flow paths, Marine Geology, 187, 119-143, 2002.

Heggland, R.: Detection of gas migration from a deep source by the use of exploration 3D seismic data, Marine Geology, 137, 41-47, 1997.

Hensen, C., Zabel, M., Pfeifer, K., Schwenk, T., Kasten, S., Riedinger, N., Schulz, H. D., and Boetius, A.: Control of sulfate pore-water profiles by sedimentary events and the significance

of anaerobic oxidation of methane for the burial of sulfur in marine sediments, Geochimica et Cosmochimica Acta, 67, 2631-2647, 2003.

Hovland, M., & Sommerville, J. H.: Characteristics of two natural gas seepages in the North Sea. Marine and Petroleum Geology, 2(4), 319-326, 1985.

Hovland, M.: On the self-sealing nature of marine seeps, Continental Shelf Research, 22, 2387-2394, 2002.

Hovland, M., & Svensen, H.: Submarine pingoes: Indicators of shallow gas hydrates in a pockmark at Nyegga, Norwegian Sea. Marine Geology, 228, 15-23, 2006.

Hovland, M., Jensen, S., and Fichler, C.: Methane and minor oil macro-seep systems — Their complexity and environmental significance, Marine Geology, 332–334, 163-173, 2012.

James, A. T.: Correlation of reservoired gases using the carbon isotopic compositions of wet gas components (1), AAPG bulletin, 74, 1441-1458, 1990.

James, R. H., Allen, D. E., and Seyfried, W.: An experimental study of alteration of oceanic crust and terrigenous sediments at moderate temperatures (51 to 350 °C): Insights as to chemical processes in near-shore ridge-flank hydrothermal systems, Geochimica et Cosmochimica Acta, 67, 681-691, 2003.

Judd, A. and Hovland, M.: Seabed Fluid Flow. The impact on geology, biology and the marine environment, Cambridge University Press. , 2009.

Justwan, H. and Dahl, B.: Quantitative hydrocarbon potential mapping and organofacies study in the Greater Balder Area, Norwegian North Sea, 2005, 1317-1329.

Karstens, J. and Berndt, C.: Seismic chimneys in the Southern Viking Graben–Implications for palaeo fluid migration and overpressure evolution, Earth and Planetary Science Letters, 412, 88-100, 2015.

Krämer, K., Holler, P., Herbst, G., Bratek, A., Ahmerkamp, S., Neumann, A., Bartholomä, A., van Beusekom, J.E.E., Holtappels, M. and Winter, C.: Abrupt emergence of a large pockmark field in the German Bight, southeastern North Sea. Scientific Reports 7, 5150, 2017

Kvenvolden, K. A. and Rogers, B. W.: Gaia's breath—global methane exhalations, Marine and Petroleum Geology, 22, 579-590, 2005.

Landschulze, K. and Pedersen, R.: Caprock integrity for offshore CO_2 storage in the Norwegian North Sea-Seismic investigation of a soft sediment seafloor fracture, AGU Fall Meeting, San Fransisco, USA, 2013.

Landschulze, K., Tveranger, J., and Pedersen, R.: Characterization of Shallow Seal Complexes for CO_2 Storage Sites–Example from the Greater Sleipner Area, 2014.

Lichtschlag, A., Felden, J., Brüchert, V., Boetius, A., and De Beer, D.: Geochemical processes and chemosynthetic primary production in different thiotrophic mats of the Håkon Mosby Mud Volcano (Barents Sea), Limnol Oceanogr, 2010.

Lonergan, L., Maidment, S. C., and Collier, J. S.: Pleistocene subglacial tunnel valleys in the central North Sea basin: 3-D morphology and evolution, Journal of Quaternary Science, 21, 891-903, 2006.

Luff, R. and Wallmann, K.: Fluid flow, methane fluxes, carbonate precipitation and biogeochemical turnover in gas hydrate-bearing sediments at Hydrate Ridge, Cascadia

Margin: numerical modeling and mass balances, Geochimica et Cosmochimica Acta, 67, 3403-3421, 2003.

Mattey, D., Lowry, D., Duffet, J., Fisher, R., Hodge, E., and Frisia, S.: A 53 year seasonally resolved oxygen and carbon isotope record from a modern Gibraltar speleothem: Reconstructed drip water and relationship to local precipitation, Earth and Planetary Science Letters, 269, 80-95, 2008.

McArthur, J., Howarth, R., and Bailey, T.: Strontium isotope stratigraphy: LOWESS version 3: best fit to the marine Sr-isotope curve for 0–509 Ma and accompanying look-up table for deriving numerical age, The Journal of Geology, 109, 155-170, 2001.

McGinnis, D. F., Greinert, J., Artemov, Y., Beaubien, S., and Wüest, A.: Fate of rising methane bubbles in stratified waters: How much methane reaches the atmosphere?, Journal of Geophysical Research: Oceans, 111, 2006.

Mokadem, F., Parkinson, I. J., Hathorne, E. C., Anand, P., Allen, J. T., and Burton, K. W.: High-precision radiogenic strontium isotope measurements of the modern and glacial ocean: Limits on glacial–interglacial variations in continental weathering, Earth and Planetary Science Letters, 415, 111-120, 2015.

Nicoll, G. D.: Evaluation of the Nordland Group overburden as an effective seal for the Sleipner CO_2 storage site (offshore Norway) using analytical and stochastic modelling techniques, 2012. University of Edinburgh, 2012

Niemann, H., Elvert, M., Hovland, M., Orcutt, B., Judd, A., Suck, I., Gutt, J., Joye, S., Damm, E., and Finster, K.: Methane emission and consumption at a North Sea gas seep (Tommeliten area), Biogeosciences Discussions, 2, 1197-1241, 2005.

Pedersen, R., Blomberg, A., Landschulze, K., Baumberger, T., Oekland, I., Reigstad, L., Gracias, N., Moerkved, P., Stensland, A., and Lilley, M.: Discovery of 3 km long seafloor fracture system in the Central North Sea, AGU Fall Meeting, San Fransisco, USA, 2013.

Pierre, C., Bayon, G., Blanc-Valleron, M.-M., Mascle, J., and Dupré, S.: Authigenic carbonates related to active seepage of methane-rich hot brines at the Cheops mud volcano, Menes caldera (Nile deep-sea fan, eastern Mediterranean Sea), Geo-Marine Letters, 34, 253-267, 2014.

Praeg, D.: Seismic imaging of mid-Pleistocene tunnel-valleys in the North Sea Basin—high resolution from low frequencies, Journal of Applied Geophysics, 53, 273-298, 2003.

Quinn, R., Bull, J., and Dix, J.: Optimal processing of marine high-resolution seismic reflection (Chirp) data, Marine Geophysical Researches, 20, 13-20, 1998.

Reeburgh, W. S.: Oceanic methane biogeochemistry. Chemical reviews, 107(2), 486-513, 2007.

Sauer, S., Knies, J., Lepland, A., Chand, S., Eichinger, F., & Schubert, C. J.: Hydrocarbon sources of cold seeps off the Vesterålen coast, northern Norway. Chemical Geology, 417, 371-382, 2015.

Schroot, B. M., Klaver, G. T., and Schüttenhelm, R. T.: Surface and subsurface expressions of gas seepage to the seabed—examples from the Southern North Sea, Marine and Petroleum Geology, 22, 499-515, 2005.

Schwietzke, S., Sherwood, O. A., Bruhwiler, L. M., Miller, J. B., Etiope, G., Dlugokencky, E. J., Michel, S. E., Arling, V. A., Vaughn, B. H., and White, J. W.: Upward revision of global fossil fuel methane emissions based on isotope database, Nature, 538, 88-91, 2016.

Sauter, E. J., Muyakshin, S. I., Charlou, J.-L., Schlüter, M., Boetius, A., Jerosch, K., Damm, E., Foucher, J.-P., and Klages, M.: Methane discharge from a deep-sea submarine mud volcano into the upper water column by gas hydrate-coated methane bubbles, Earth and Planetary Science Letters, 243, 354-365, 2006.

Sejrup, H., Larsen, E., Landvik, J., King, E., Haflidason, H., and Nesje, A.: Quaternary glaciations in southern Fennoscandia: evidence from southwestern Norway and the northern North Sea region, Quaternary Science Reviews, 19, 667-685, 2000.

Sommer, S., Linke, P., Pfannkuche, O., Schleicher, T., Schneider, J., Reitz, A., Haeckel, M., Flögel, S., and Hensen, C.: Seabed methane emissions and the habitat of frenulate tubeworms on the Captain Arutyunov mud volcano (Gulf of Cadiz), Marine Ecology Progress Series, 382, 69-86, 2009.

Sommer, S., Schmidt, M., and Linke, P.: Continuous inline mapping of a dissolved methane plume at a blowout site in the Central North Sea UK using a membrane inlet mass spectrometer–Water column stratification impedes immediate methane release into the atmosphere, Marine and Petroleum Geology, 68, 766-775, 2015.

Skarke, A., Ruppel, C., Kodis, M., Brothers, D., and Lobecker, E.: Widespread methane leakage from the sea floor on the northern US Atlantic margin, Nature Geoscience, 7, 657-661, 2014.

Swinnerton, J. W., and Linnenbom, V. J.: Determination of the C1 to C4 hydrocarbons in sea water by gas chromatography. Journal of Gas Chromatography 5, 570-573, 1967.

Torres, M. E., Bohrmann, G., and Suess, E.: Authigenic barites and fluxes of barium associated with fluid seeps in the Peru subduction zone, Earth and Planetary Science Letters, 144, 469-481, 1996.

Tóth, Z., Spieß, V., and Jensen, J.: Seismo-acoustic signatures of shallow free gas in the Bornholm Basin, Baltic Sea, Continental Shelf Research, 88, 228-239, 2014.

Vanneste, M., Sultan, N., Garziglia, S., Forsberg, C. F., and L'Heureux, J.-S.: Seafloor instabilities and sediment deformation processes: the need for integrated, multi-disciplinary investigations, Marine Geology, 352, 183-214, 2014.

Vielstädte, L., Karstens, J., Haeckel, M., Schmidt, M., Linke, P., Reimann, S., Liebetrau, V., McGinnis, D. F., and Wallmann, K.: Quantification of methane emissions at abandoned gas wells in the Central North Sea, Marine and Petroleum Geology, 2015.

von Deimling, J. S., Linke, P., Schmidt, M., and Rehder, G.: Ongoing methane discharge at well site 22/4b (North Sea) and discovery of a spiral vortex bubble plume motion, Marine and Petroleum Geology, 68, 718-730, 2015.

von Deimling, J. S., Rehder, G., Greinert, J., McGinnnis, D., Boetius, A., and Linke, P.: Quantification of seep-related methane gas emissions at Tommeliten, North Sea, Continental Shelf Research, 31, 867-878, 2011.

Wiggins, S. M., Leifer, I., Linke, P., and Hildebrand, J. A.: Long-term acoustic monitoring at North Sea well site 22/4b, Marine and Petroleum Geology, 68, 776-788, 2015.

Wimpenny, J., Gíslason, S. R., James, R. H., Gannoun, A., Von Strandmann, P. A. P., and Burton, K. W.: The behaviour of Li and Mg isotopes during primary phase dissolution and

secondary mineral formation in basalt, Geochimica et Cosmochimica Acta, 74, 5259-5279, 2010.

Wiprut, D. and Zoback, M. D.: Fault reactivation and fluid flow along a previously dormant normal fault in the northern North Sea, Geology, 28, 595-598, 2000.

Yamamoto, S., Alcauskas, J. B., and Crozier, T. E.: Solubility of methane in distilled water and seawater, Journal of Chemical & Engineering Data, 21, 78-80, 1976.

Tables

Table 1: Geochemical composition of Utsira Formation waters (well 15/9-F-07 and 15/9-F-09) compared to the composition of porewaters in the upper 3 m of the background sites (average of VC01, VC04, VC12, VC15, VC16, VC20, VC24) and advected fluids (VC04, VC08, VC14, VC28). n.d.=not determined, b.d.=below detection. $*^{87}Sr/^{86}Sr$ data for formation fluids are from an earlier sampling campaign in 2011.

Species	Utsira Formation water 15/9-F-07	Utsira Formation water 15/9-F-09	Background sediment porewater	Hugin Fracture porewater
Cations				
Li (μmol kg^{-1})	424	341	27 ±3	31
B (μmol kg^{-1})	1557	1449	400 ±51	475
Na (mmol kg^{-1})	491	485	474 ±50	338
Mg (mmol kg^{-1})	24	22	53 ±6	33.5
Ca (mmol kg^{-1})	11.4	10.1	12.3 ±1.3	5.5
Rb (μmol kg^{-1})	0.9	0.8	n.d.	n.d.
Sr (μmol kg^{-1})	104	99	88 ±9	61
Ba (μmol kg^{-1})	4.5	2.1	0.2 ±0.2	7.6
Anions				
Cl (mmol L^{-1})	533	518	540 ±65	247
Br (μmol L^{-1})	1273	1208	870 ±108	400
SO$_4$ (mmol L^{-1})	0.05	0.01	27.48 ±3.36	0.28
Carbonate System				
pH	7	7	n.d.	n.d.
DIC (mmol L^{-1})	16.6	18.2	2.6 ±0.1	13.0
TA (mmol L^{-1})	16.2	19.3	2.6 ±0.3	19.5
Nutrients				
Phosphate (μmol L^{-1})	0.7	0.8	6 ±4	35
Silicate (μmol L^{-1})	274	317	100 ±38	310
NO$_x$ (μmol L^{-1})	b.d.	b.d	8 ±6	28
Other parameters				
Sulfide (μmol L^{-1})	b.d	b.d	b.d	5971
T (°C)	29.5	29.3	n.d.	n.d.
$^{87}Sr/^{86}Sr*$	0.70924	0.70924	0.70916	0.70928

Figure Captions

Figure 1: (a) Map of the area, (b) with side-scan imagery of the Hugin Fracture Area and the abandoned well 16/4-2, (c) the Hugin Fracture detailed area and (d) an interpretation of the detailed area. The two main fault segments and the fault bend location are indicated. The Hugin Fracture is indicated by the solid red line; the possible surficial fault extent is indicated by the red dotted line. The abandoned well 16/4-2 is indicated by the red star.

Figure 2: Autosub 6000 pictures acquired within the Hugin Fracture area (Dive M62, flying altitude 3 m). The seabed sediments mainly comprise sandy sediments (a), and shell hashes (white backscatter) (b), however locally along the Hugin Fracture, and well 16/4-2 where there is increased fluid flow activity bacterial mats and reduced sediments (dark spotting) are seen (c-j). The abandoned well 16/4-2 is indicated by the red star.
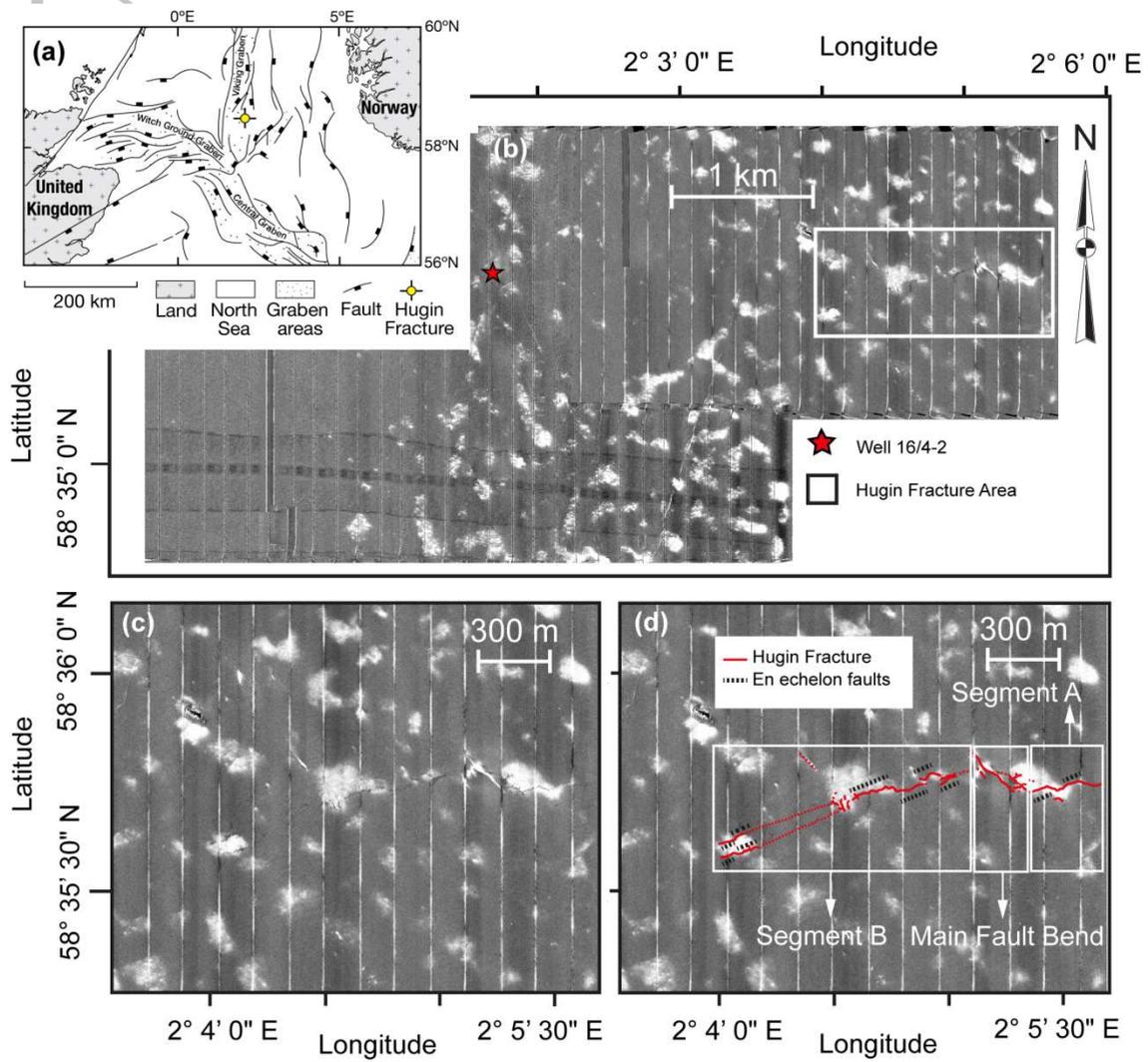
Figure 3: Autosub AUV Chirp reflection profiles exhibiting acoustic amplitude anomalies within the top 5 m of the sub-surface. (a) Profile across the Hugin Fracture, with enhanced reflectivity in the down-thrown side; (b) zoomed wiggle trace view showing enhanced reflectivity.

Figure 4: RMS seismic amplitude anomalies from Chirp seismic reflection data within the Hugin Fracture area. The RMS amplitude is calculated from the seabed return down to 3 ms Two Way Time below the seabed. Seismic amplitude anomalies are detected along the Hugin Fracture (solid line) and at the abandoned well site (star). Locations of the possible surficial fault extent of the Hugin Fracture (black dotted line), and VC locations (dots) are shown.
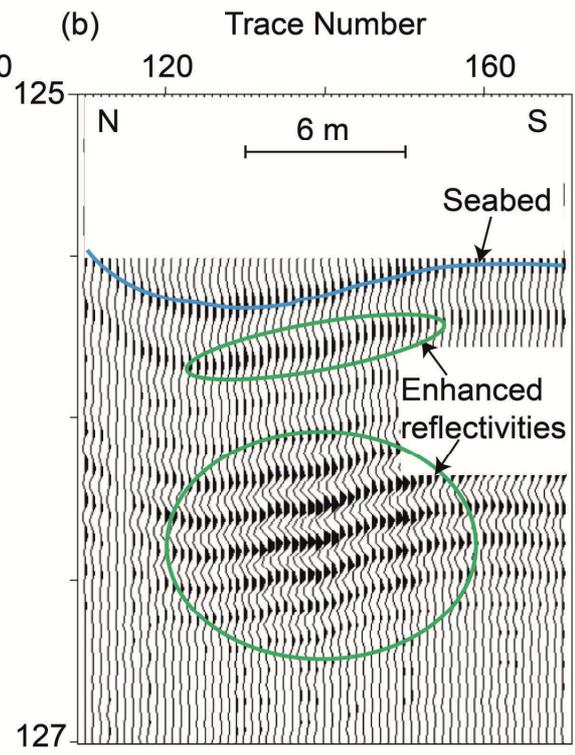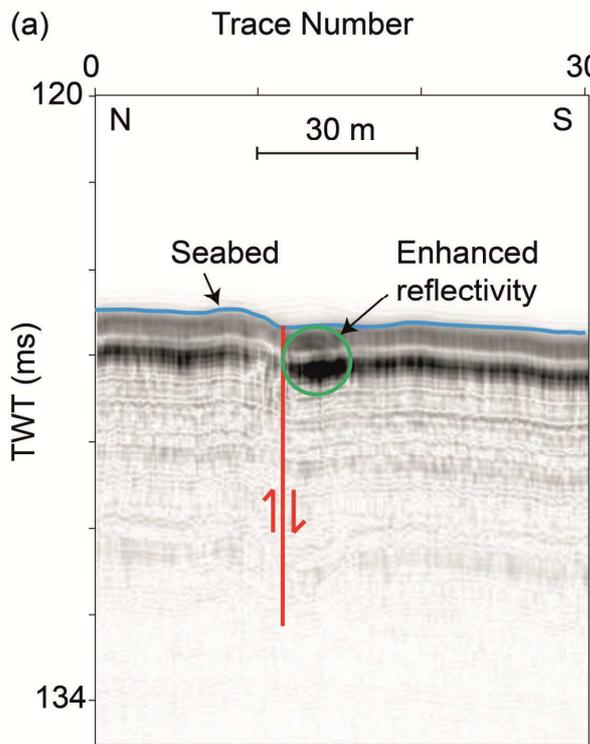
Figure 5: Methane concentrations in the water column: (a) Transect from the southern part of the area south of the Hugin Fracture up to the Hugin Fracture in the North; (b) W-E transect following the Hugin Fracture surface expression.

Figure 6: Composition of sediments and sediment porewaters in areas with active fluid flow along the Hugin Fracture; (a) VC08, (b) VC10, (c) VC14, (d) VC28) and a background site close to the Hugin Fracture; (e) VC04. The dashed vertical lines show the concentration measured in the background site. Note different scales for sulfide. Sediment and porewater geochemistry of other cores taken outside the Hugin Fracture, close to the abandoned well and in the area south of the Hugin Fracture are displayed in Figure S2. All data are deposited in the Earth System database www.PANGAEA.de (https://doi.org/10.1594/PANGAEA.883560).
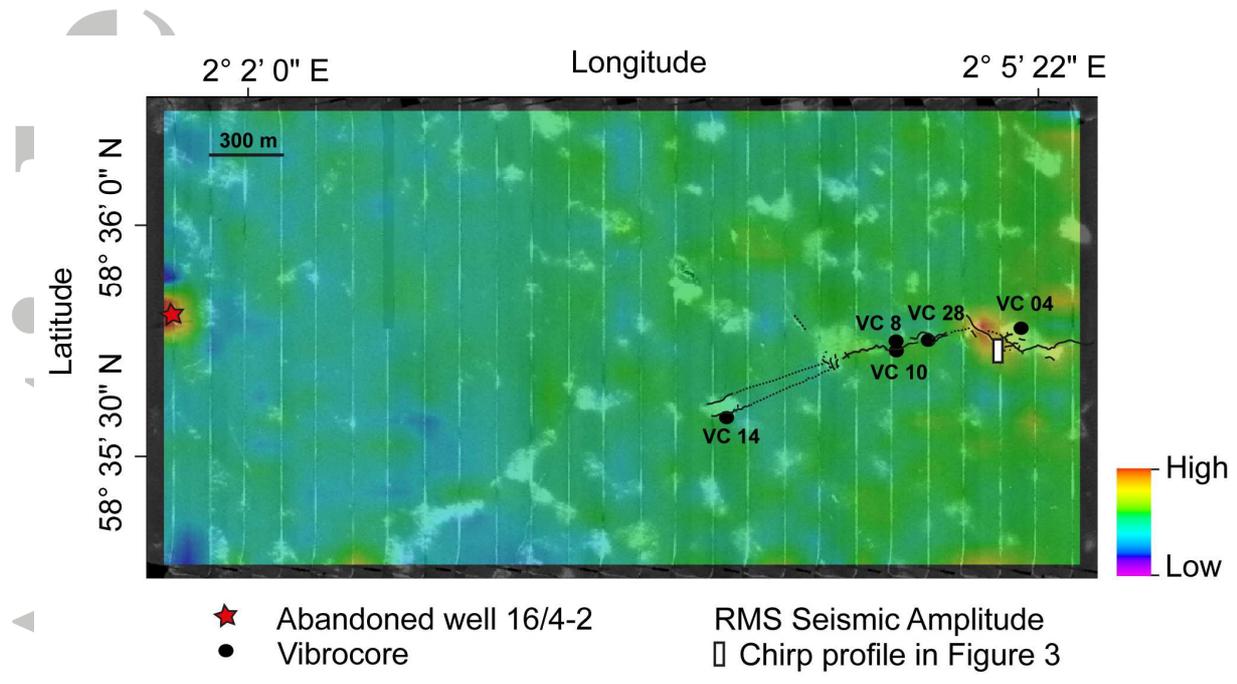
Figure 7: Sr isotope (^{87}Sr/^{86}Sr) variation with depth in sediment porewaters. VC10, VC08 and VC14 are characterized by fluid flow; in VC08 methane is present in the upper 1 m and in VC10 methane is absent; in both cores sulfide concentrations are relatively high. In VC14 methane and sulfide concentrations are low. VC04 is the background site. Seawater ^{87}Sr/^{86}Sr is shown by the dashed line (Mokadem et al., 2015) and the ^{87}Sr/^{86}Sr composition of Utsira Formation waters is shown by the dotted line.
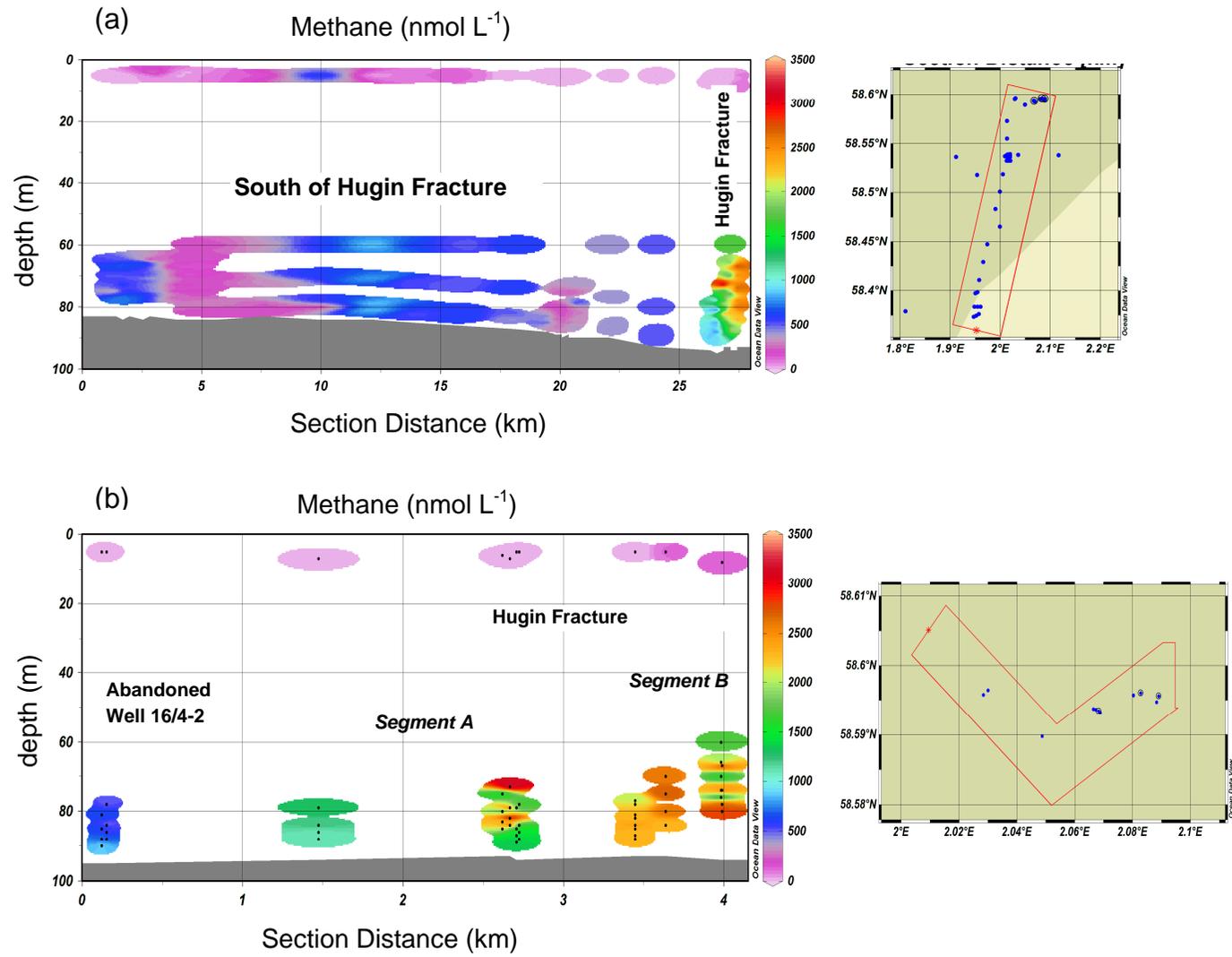
Longitude

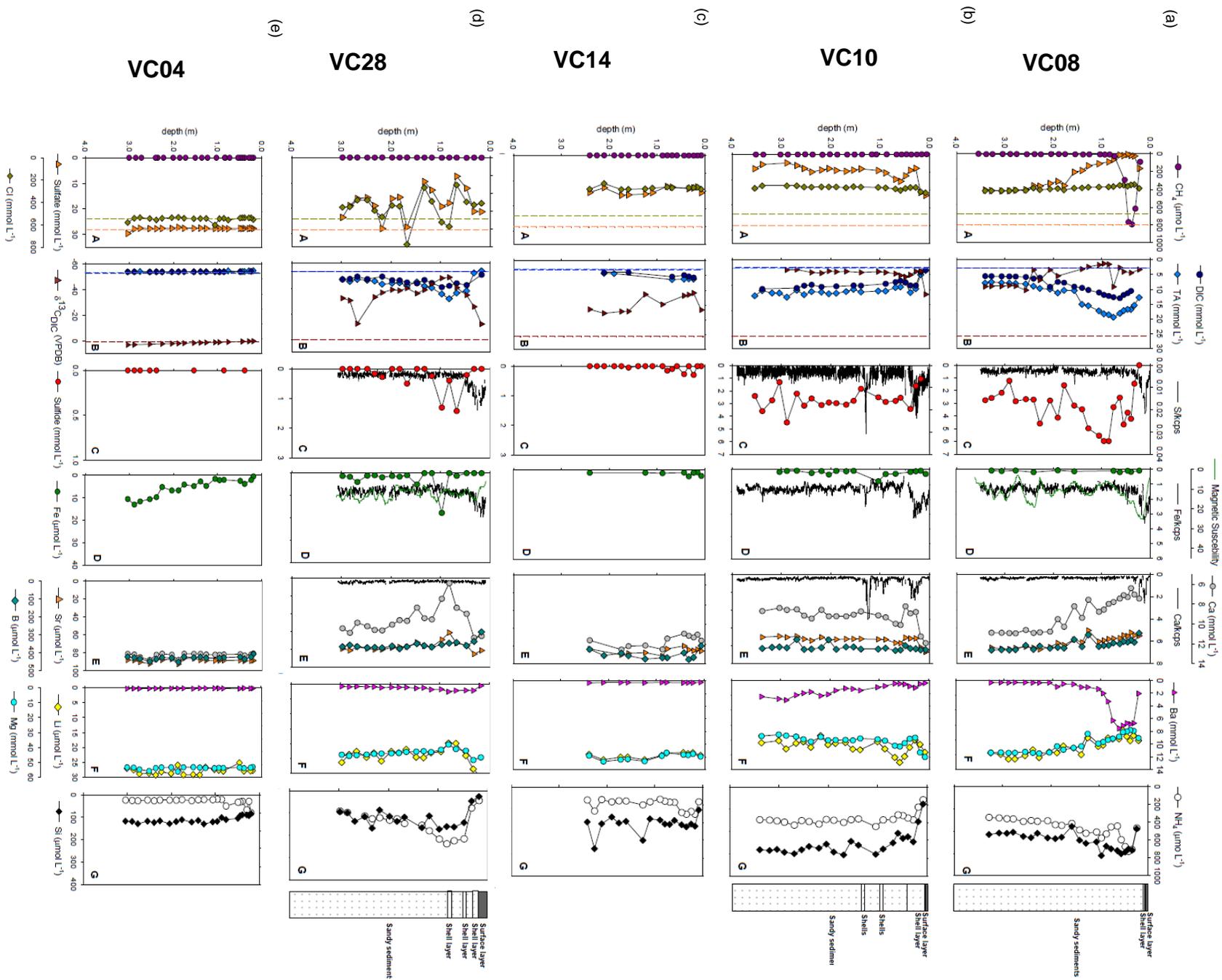Latitude

N

58° 36' 30" N

58° 34' 30" N

(a)

(b)

(c)

(d)

(e)

(f)

(g)

(h)

(i)

(j)

300 m

1.2 m

1.4 m

★ Well 16/4-2 — Hugin Fracture

★ Autosub 6000 picture sampling points

2° 2' 0" E   2° 6' 0" E

Longitude

2° 2' 0" E   2° 5' 22" E

Latitude

58° 36' 0" N
58° 35' 30" N

300 m

VC 8   VC 28   VC 04
VC 10
VC 14

High

Low

★ Abandoned well 16/4-2   RMS Seismic Amplitude
● Vibrocore   ▯ Chirp profile in Figure 3

(a) Methane (nmol L^{-1})

South of Hugin Fracture

Hugin Fracture

depth (m)

Section Distance (km)

(b) Methane (nmol L^{-1})

Hugin Fracture

Abandoned
Well 16/4-2

Segment A

Segment B

depth (m)

Section Distance (km)